

## Dye-sensitized Solar Cell (DSSC) Utilizing TiO<sub>2</sub> Films Prepared via Microwave Irradiation Technique: Effect of TiO<sub>2</sub> Growth Time

M.Y.A. Rahman<sup>1\*</sup>, L. Roza<sup>2</sup>, S.A.M. Samsuri<sup>1</sup>, A.A. Umar<sup>1</sup> and M.M. Salleh<sup>1</sup>

<sup>1</sup>Institute of Microengineering and Nanoelectronics (IMEN), Universiti Kebangsaan Malaysia, 43600, Bangi, Selangor, Malaysia

<sup>2</sup>Jurusan Fisika, Fakultas Keguruan dan Ilmu Pendidikan, Universitas Muhammadiyah Prof. Dr. Hamka, 13730, Jakarta Timur, Indonesia

Received: December 18, 2016, Accepted: March 01, 2017, Available online: May 10, 2017

**Abstract:** This paper is concerned with the influence of TiO<sub>2</sub> films growth time on the performance parameters of a DSSC. The films were prepared via microwave irradiation technique by varying growth times, 3, 5, 7, 10 and 12 minutes. The XRD results reveal that anatase phase exists at (101) and (004) plane with the biggest crystallite size was obtained at the growth time of 3 minutes. The FESEM images show that morphological shape of nanotablet was obtained at shorter irradiation time. The particle size and thickness were found to increase with growth time. However, the particle density decreases with growth time. The uncoated dye and coated dye samples grown at 10 minutes possesses the highest optical absorption and the broadest absorption window. The DSSC utilizing the TiO<sub>2</sub> samples did not show rectification property. It was found that the photovoltaic parameters of the DSSC are greatly influenced by the growth time of TiO<sub>2</sub> films. The DSSC utilizing the sample prepared for 10 minutes demonstrated the highest  $J_{SC}$ ,  $V_{oc}$  and  $\eta$  of 2.60 mA cm<sup>-2</sup>, 0.62 V and 0.86%, respectively due to broadest absorption window, the highest recombination resistance ( $R_{cr}$ ) and longest charge carrier lifetime ( $\tau$ ).

**Keywords:** dye-sensitized solar cell, microwave, photoanode, titanium dioxide

### 1. INTRODUCTION

Photoanode in DSSC acts as a medium to collect electrons injected by dye molecules upon light illumination on the device. Wide band gap metal oxide semiconductors are normally used in DSSC such as TiO<sub>2</sub>, ZnO [1,2], SnO<sub>2</sub> [3], WO<sub>3</sub> [4], Nb<sub>2</sub>O<sub>5</sub> [5] and Zn<sub>2</sub>SnO<sub>4</sub> [6]. The bandgap of TiO<sub>2</sub>, ZnO, SnO<sub>2</sub>, WO<sub>3</sub>, Nb<sub>2</sub>O<sub>5</sub> and Zn<sub>2</sub>SnO<sub>4</sub> are 3.20, 3.20, 3.80, 2.60, 3.40 and 3.60 eV, respectively. Among these materials, TiO<sub>2</sub> or titania is the most popular photoanode in DSSC since it is the most stable material, cheap, easily available and non-toxic. There are various techniques have been reported in preparing TiO<sub>2</sub> films on various substrates such as screen-printing [7], RF magnetron sputtering [8], pulsed laser ablation [9], spray pyrolysis [10], sol-gel [11], liquid phase deposition [12] and hydrothermal [13].

In this work, TiO<sub>2</sub> films have been prepared on ITO substrate via microwave irradiation technique [14]. Microwave irradiation technique has been chose since it produces thin films for short duration at low temperature. The originality of this work is the

addition of boric acid and surfactant, CTAB into a growth solution in order to alter the morphology of TiO<sub>2</sub> films. The objective of this work is the investigation of the effect of TiO<sub>2</sub> growth time on the properties of the films such as structure, morphology and optical absorption. These properties were then linked to the performance parameters of DSSC. The growth time was also correlated with EIS data such as  $R_b$ ,  $R_{cr}$  and  $\tau$ .

### 2. EXPERIMENTAL

#### 2.1. Preparation of TiO<sub>2</sub> nanostructures

TiO<sub>2</sub> films nanostructures were grown on ITO substrate by using a chemical wet microwave-assisted method. A cleaned indium tin oxide (ITO) substrate purchased from Zhuhai Kaivo Electronic with a sheet resistance of ~10 cm/square was immersed into a growth solution consisting of 5 mL of 0.1 M ammonium hexafluorotitanate, (NH<sub>4</sub>)<sub>2</sub>TiF<sub>6</sub> (Sigma Aldrich), 5 mL of 0.2 M H<sub>3</sub>BO<sub>3</sub> (R&M Chemical) and 0.1 mL of 0.1 M CTAB (Sigma Aldrich) surfactant. The substrate was vertically suspended in the solution and then transferred into a microwave oven (Panasonic Home Appliances, NN-GD577M, 1100 W, 2.45 GHz) and heated at 180 W for 3, 5, 7, 10 and 12 minutes, respec-

\*To whom correspondence should be addressed: Email: mohd.yusri@ukm.edu.my  
Phone: 60389118543

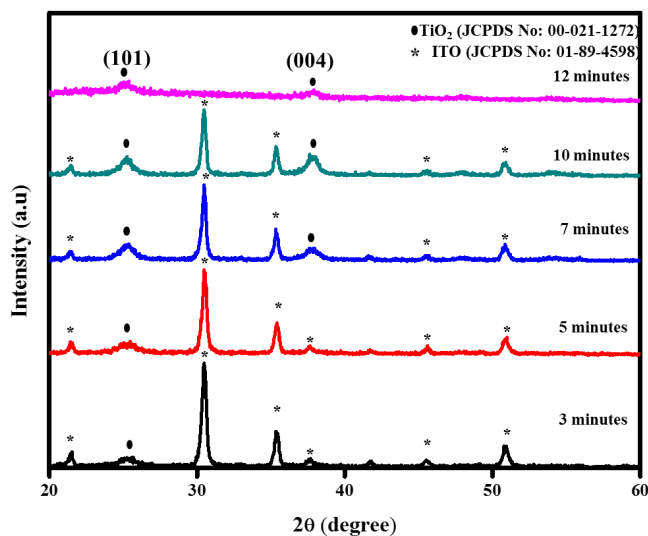


Figure 1. XRD patterns of TiO<sub>2</sub> films prepared at various growth times

tively. The growth temperature was in the range 100–150 °C. The preparation of TiO<sub>2</sub> nanostructures was completed by rinsing the sample with adequate amount of deionized water and then subjected to an annealing process at 400 °C for 30 minutes in air.

## 2.2. Fabrication and characterization of DSSC

TiO<sub>2</sub> nanostructures grown on ITO were dipped into 0.5 mM ethanolic solution of dye N719 (Sigma-Aldrich) at 50 °C for 15 hours. The sample was rinsed with ethanol and dried with nitrogen gas flow. Counter electrodes for these DSSCs were prepared by the deposition of platinum layer on ITO substrate using sputtering method. The dye coated TiO<sub>2</sub> film and the counter electrode were sealed using Surlyn film of thickness 100 μm. The DSSC consisting of TiO<sub>2</sub> films as photoanode and platinum film as counter electrode with iodine electrolyte were fabricated. The TiO<sub>2</sub> films were prepared on ITO substrate via liquid phase deposition technique. An electrolyte containing 0.5 M LiI/0.05 M I<sub>2</sub>/0.5 M TBP in acetonitrile was used as a redox couple. A DSSC was fabricated by sandwiching the parafilm between TiO<sub>2</sub> film and platinum counter electrode film. The electrolyte, idolyte-Z50 (Solaronix) was injected into a space between N719 coated TiO<sub>2</sub> film and platinum counter electrode via a capillary action.

The photovoltaic performance of the DSSC was investigated by current–voltage measurement under 100 mW cm<sup>-2</sup> tungsten light using Keithley 237 source measurement unit. The dark current was also observed by the same measurement set-up. The illuminated area of the cell was 0.23 cm<sup>2</sup>. The electrochemical impedance spectroscopy (EIS) technique was also performed to study the bulk resistance ( $R_b$ ), the recombination resistance ( $R_{cr}$ ) and charge carrier lifetime at the applied voltage of 0.4 V.

## 3. RESULTS AND DISCUSSION

Fig. 1 shows the XRD spectra of the TiO<sub>2</sub> film samples with various growth times. The spectra show two dominant anatase peaks at the (101), and (004) planes for all samples, corresponding

with the diffraction angles, 25.4 and 38.2°, respectively. These results agree well with the data reported in [15]. The diffraction peak at 21.3, 31.2, 37.1, 47.0 and 51.5° are referred to ITO substrate. This result is consistent with that reported in [16]. It is found that the peak intensity of ITO at 31.2° decreases with growth time since the thickness of TiO<sub>2</sub> film increases with growth time as illustrated in Table 1. The thicker film allows weaker x-ray signal to penetrate, causing lower peak intensity. Also, from the spectra, it was found that the phase structure of TiO<sub>2</sub> does not change with its growth time. The crystallite size at (101) plane for each sample is presented in Table 1. From the table, it is observed that the crystallite size decreases with growth time and increases at the optimum growth time of 10 minutes.

Fig. 2 shows the top view FESEM images of TiO<sub>2</sub> films prepared at various growth times. At 3 minutes growth time, the morphological shape of TiO<sub>2</sub> film is nanotablet with the particle size and density is 129 nm and 30 particle/μm<sup>2</sup>, respectively as illustrated in Table 1. The morphology is inhomogeneous and the particle distribution is not packed since there are a lot of spaces between the particles. Once the growth time was increased to 5 minutes, the size of nanotablet becomes bigger. On the other hand, the particle density decreases as shown in Table 1. Further increment of growth time to 7 minutes causing shape of the particle transforms into nanosheet. The particle size increases drastically to 421 nm. However, the particle density drops to 5 particle/μm<sup>2</sup>. The shape of particle was found to change from nanosheet to compact nanoparticle when the growth time was further increased to 10 minutes. However, the particle size and density cannot be estimated since the particle distribution is very compact. At the growth time of 12 minutes, cracked nanoparticle film has been observed since 12 minutes is not an appropriate time to grow nanoparticle via microwave technique. The morphology becomes cracked due to the compact nanoparticles touch each other and increases the surface tension of the sample [17].

Fig. 3 shows the cross-sectional view of FESEM images of TiO<sub>2</sub> films prepared at various growth times. The images clearly show two layers with different materials, namely, TiO<sub>2</sub> film and ITO film forming the sample. The sample grown at 3 minutes shows the smoothest surface, while that prepared for 5 and 12 minutes possess rough surface since they display many humps on ITO layer. The thickness of TiO<sub>2</sub> film is presented in Table 1 and it is found that the thickness increases with growth time. The increase of the thickness with growth time is due to the increase in the amount of TiO<sub>2</sub> deposited on ITO substrate as the growth time is increased.

Table 1. Crystallite size, particle size, particle density and thickness of the samples at various growth temperatures

Sample (minutes)	Crystallite size (nm)	Particle size (nm)	Particle density (particle/μm <sup>2</sup> )	Thickness (nm)
3	16.38	129±32	30±8	105±15
5	12.11	253±47	7±1	184±45
7	12.39	421±29	5±1	225±21
10	14.44	-	-	362±19
12	13.16	-	-	369±41

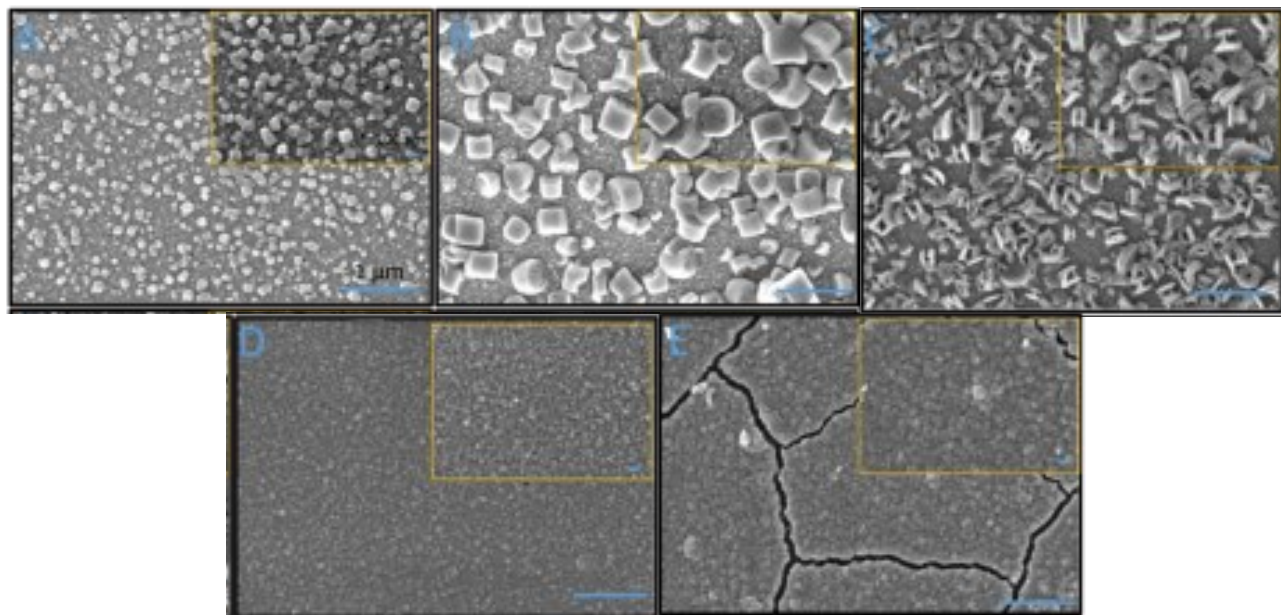


Figure 2. Top view FESEM images with the 20k magnification of TiO<sub>2</sub> films prepared at various growth times, (A) 3, (B) 5, (C) 7, (D) 10 and (E) 12 minutes. The insets are the images with the 50k magnification.

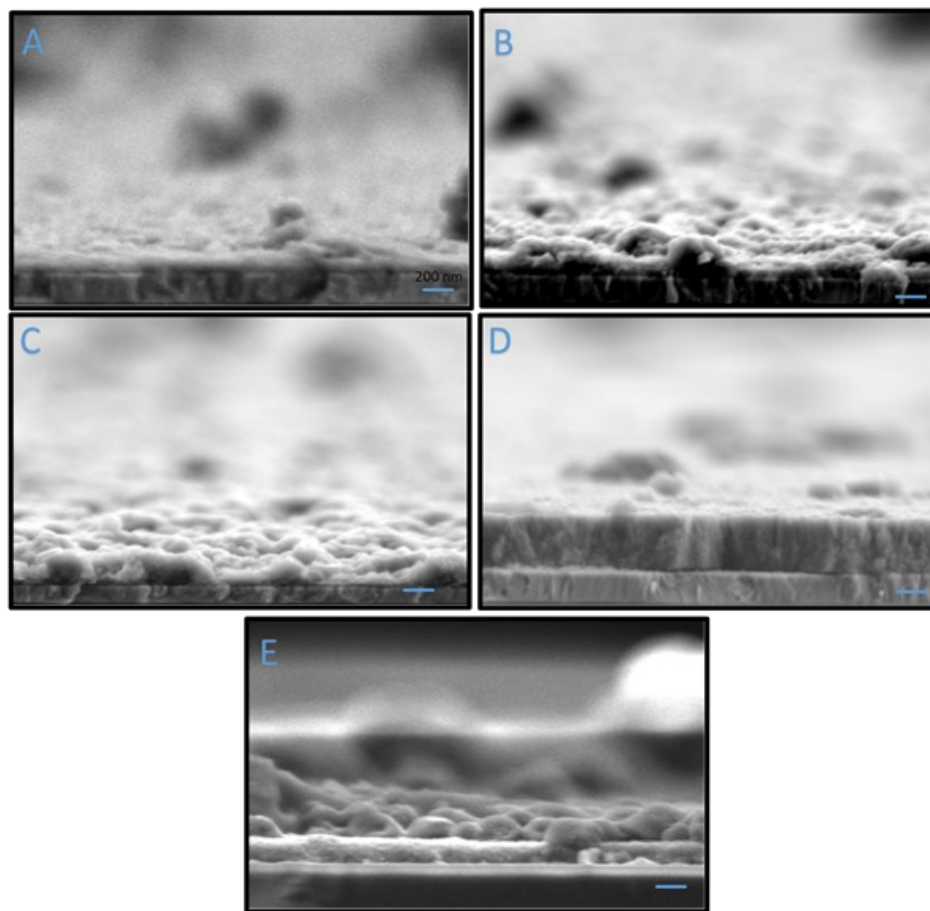


Figure 3. Cross-sectional view of FESEM images of TiO<sub>2</sub> films prepared at various growth times, (A) 3, (B) 5, (C), (D) 10 and (E) 12 minutes

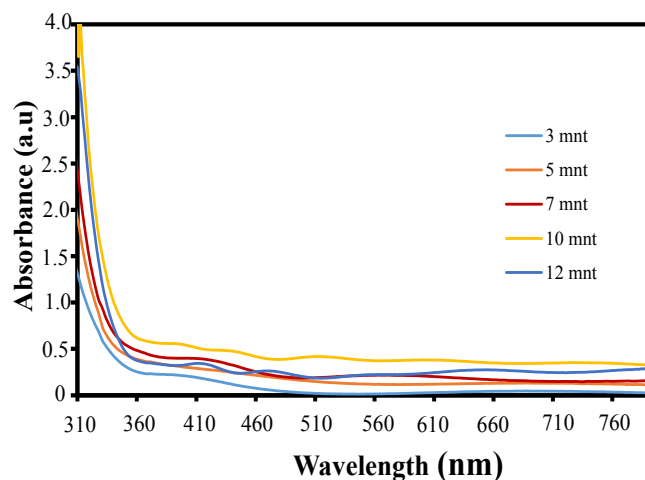


Figure 4. UV-Vis spectra of TiO<sub>2</sub> films prepared at various growth times

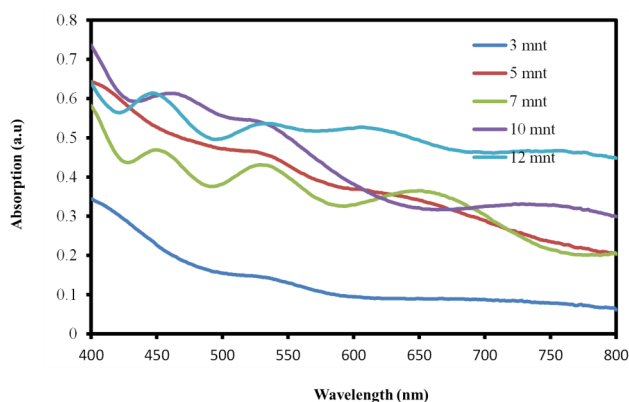


Figure 5. UV-VIS optical absorption spectra of TiO<sub>2</sub> sample prepared at various growth times after dipping dye for 15 h

Fig. 4 illustrates the UV-Vis spectra of TiO<sub>2</sub> films prepared at various growth times. According to the figure, all samples absorb more photons in ultraviolet region with low absorption in visible region since the bandgap of TiO<sub>2</sub> film is wide that is 3.37 eV. The absorption peaks are observed in ultraviolet region. The absorption window area is significantly influenced by growth time. The sample grown for 3 minutes possesses the smallest absorption window and the one prepared for 10 minutes shows the largest absorption window area.

Fig. 5 illustrates the UV-Vis spectra of TiO<sub>2</sub> films coated N719 dye prepared at various growth times. It is observed that from the spectra, all samples possess dominant absorption in visible region except the sample grown for 3 minutes that has normalized absorption of 0.34. The other samples show the normalized absorption above 0.5 as seen from Fig. 5. The sample prepared for 10 minutes shows the highest area of window absorption compared with the other samples. By comparison of the UV-Vis spectra of uncoated dye samples with those of N719 dye samples, it is confirmed the dye has shifted the optical absorption of TiO<sub>2</sub> films from ultraviolet to visible region.

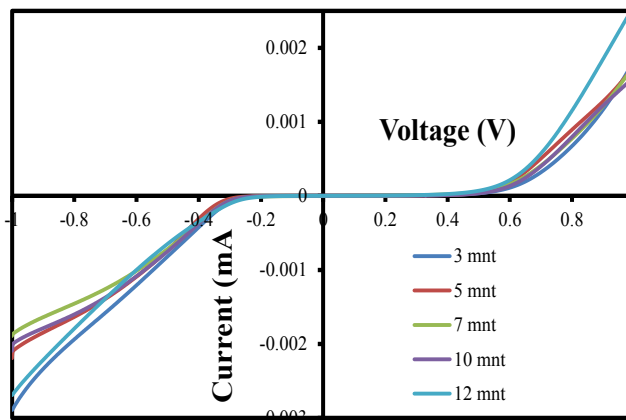


Figure 6.  $I$ - $V$  curves of the devices in dark with various TiO<sub>2</sub> growth times

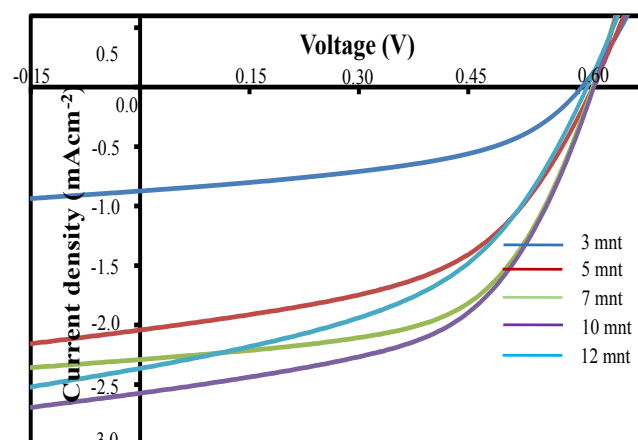


Figure 7.  $J$ - $V$  curves of the devices with various TiO<sub>2</sub> growth times under illumination of 100 mW cm<sup>-2</sup>

Fig. 6 depicts the  $I$ - $V$  curves in dark of the DSSCs utilizing the TiO<sub>2</sub> films with various growth times. It is observed that the dark current in reverse bias is slightly higher than that in forward bias for all devices. The device utilizing 10 minutes TiO<sub>2</sub> sample demonstrates the highest dark current in forward bias, while the other devices show quite similar dark current. For the dark current in reverse bias which is also called leak current, the device utilizing 7 minutes sample possesses the lowest leak current and the one utilizing 12 minute sample shows the highest leak current. It is concluded that the device does not exhibit as a rectifier as the device with 3, 5, 7 and 10 minutes have quite similar dark current in forward bias.

Fig. 7 displays the current density-voltage ( $J$ - $V$ ) curves of the DSSC utilizing the samples prepared with various growth times under 100 mW cm<sup>-2</sup> light illuminations. The photovoltaic parameters are extracted from Fig. 7 and illustrated in Table 2. The device with 10 minutes TiO<sub>2</sub> sample shows the largest area of  $J$ - $V$ , meanwhile that utilizing 3 minutes sample has the smallest area of the curve. These results indicate that the DSSC with 10 minutes samples demonstrates the highest output power and that with 3 minutes

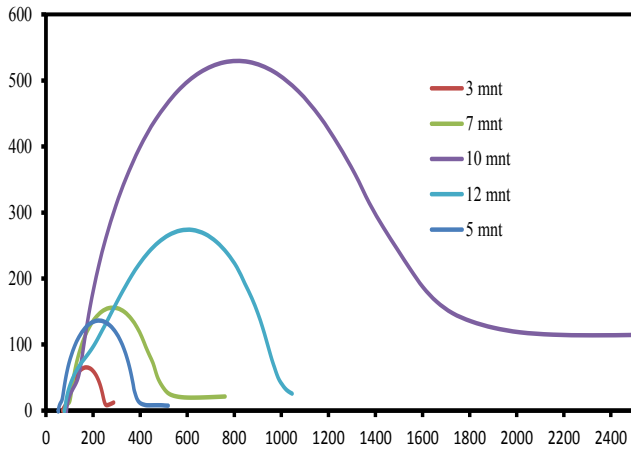


Figure 8. Nyquist plots of the DSSCs utilizing TiO<sub>2</sub> films prepared at various growth times

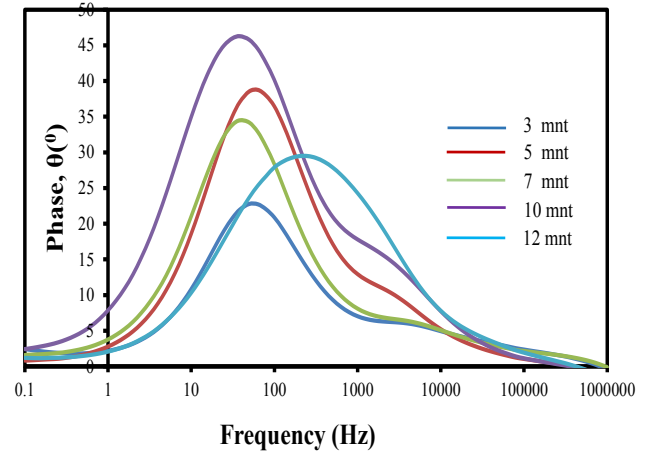


Figure 9. Bode plots of the DSSCs utilizing TiO<sub>2</sub> films prepared at various growth times

sample generates the lowest output power. It is also found that the slope of each curve is quite high, leading to small fill factor (*FF*) which is in the range 0.46-0.53 as presented in Table 2. Small *FF* is due to high output power loss which is caused by high leak current as illustrated in Fig. 6.

Fig. 8 shows Nyquist plots of the DSSC utilizing the samples with various growth times. The plots clearly show complete semi-circular curves representing the recombination resistance (*R<sub>cr</sub>*) of electron-hole. A straight line just before the semicircle represents the bulk resistance (*R<sub>b</sub>*) of the device. The device with 3 minute sample shows the smallest semicircle and the one utilizing 10 minutes sample displays the biggest semicircle denoting the 3 and 10 minutes device exhibits the lowest and the highest *R<sub>cr</sub>*, respectively. The *R<sub>b</sub>* for all devices and *R<sub>cr</sub>* for the other 3 devices are presented in Table 2.

Fig. 9 illustrates Bode plots of the devices utilizing the samples with various growth times. The plots show bell-shaped curves which are symmetry about a resonant frequency. Carrier lifetime is computed from the resonant frequencies which are taken from the peak of each curve. It is observed that 7 and 10 minutes device has the smallest resonant frequency, while that with 12 minutes sample shows the highest resonant frequency. These data signify that the device with 7 and 10 minutes have the longest carrier lifetime and the one with 12 minutes sample possesses the shortest carrier lifetime as presented in Table 2.

Table 2 illustrates the photovoltaic parameters, *R<sub>b</sub>*, *R<sub>cr</sub>* and carrier

lifetime with various growth times. According to the table, the *J<sub>sc</sub>* and *η* increase with growth time until the optimum time of 10 minutes. This trend is also seen for the *R<sub>cr</sub>* and *τ*. It can be concluded that the higher these photovoltaic parameters, the higher *R<sub>cr</sub>* and *τ*. This is consistent with the theory that the higher resistance for the recombination of electron-hole and longer carrier lifetime results in the improvement in those photovoltaic parameters. At the optimum growth time of 10 minutes, these photovoltaic parameters drop which is due to the decrement in the *R<sub>cr</sub>* and *τ* as illustrated in Table 2. On the other hand, the 3 minutes device performs the lowest *J<sub>sc</sub>* and *η* since it has the lowest *R<sub>cr</sub>* and shortest *τ* as shown in Table 2. The performance of the device in term of *J<sub>sc</sub>* and *η* is also influenced by the optical absorption of TiO<sub>2</sub> films as depicted in Fig. 5. According to the figure, 10 minute sample shows the highest peak absorption at 455 nm in visible region and 3 minute sample possesses the smallest area of window absorption. The higher peak absorption and the larger area of absorption window caused the higher those photovoltaic parameters. It is also found from the table that the *V<sub>oc</sub>* is quite similar to each other, indicating that the growth time does not affect the *V<sub>oc</sub>*.

Also, according to Table 2, the highest *η* obtained is 0.86%. It is higher than that reported in [18] that was 0.77% for the DSSC utilizing TiO<sub>2</sub> films and coumarin dye. This is because N719 dye possesses higher optical absorption than coumarin dye in visible region. However, it is lower than that reported in [19] which was 1.69% obtained from the DSSC utilizing TiO<sub>2</sub> films prepared via

Table 2. Photovoltaic parameters and EIS data of the device utilizing TiO<sub>2</sub> prepared by various growth times

Growth time (minute)	<i>V<sub>oc</sub></i> (V)	<i>J<sub>sc</sub></i> (mA cm <sup>-2</sup> )	<i>FF</i>	<i>η</i> (%)	<i>R<sub>b</sub></i> (Ω)	<i>R<sub>cr</sub></i> (Ω)	<i>τ</i> (ms)
3	0.60	0.87	0.48	0.25	20	165	2.0
5	0.62	2.04	0.50	0.63	20	400	2.0
7	0.62	2.30	0.57	0.81	20	600	3.2
10	0.62	2.60	0.53	0.86	50	2400	3.2
12	0.61	2.36	0.46	0.67	10	1000	0.5

liquid phase deposition technique. It is also lower than that reported in [18] that was 5.36% for the DSSC utilizing N719 dye. The lower  $\eta$  of this work compared with that reported in [18, 19] might be due to the thickness of TiO<sub>2</sub> films in this work is smaller than that in [18,19]. The thicker films provide more number of free electron-hole pairs upon light illumination.

#### 4. CONCLUSIONS

The films have successfully been prepared via microwave irradiation technique at low temperature for short period, 3-12 minutes. The XRD analysis confirms the presence of anatase phase for all samples with variation of growth times. The FESEM images reveal that morphological shape of nanotablet was obtained at shorter irradiation time, followed by nanosheet and nanoparticle at longer growth time. The particle size and thickness increase with growth time but the particle density decreases with growth time. The uncoated dye and coated dye samples grown at 10 minutes possesses the highest optical absorption and the broadest absorption window. The DSSC utilizing the sample prepared for 10 minutes demonstrated the highest performance with the  $J_{SC}$ ,  $V_{oc}$  and  $\eta$  of 2.60 mA cm<sup>-2</sup>, 0.62 V and 0.86%, respectively due to broadest absorption window, the highest recombination resistance ( $R_{cr}$ ) and longest charge carrier lifetime ( $\tau$ ).

#### 5. ACKNOWLEDGMENTS

This work was supported by Universiti Kebangsaan Malaysia (UKM) under research grant DLP 2015-003 and GUP-2016-013.

#### REFERENCES

- [1] S.H Ko, D. Lee, H.W. Kang, K.H. Nam, J.Y. Yeo, S.J. Hong, Nano Lett., 11, 666 (2011).
- [2] M.Y.A. Rahman, A.A. Umar, R. Taslim, M.M. Salleh, Electrochim. Acta, 88, 639 (2013).
- [3] S. Gubbala, V. Chakrapani, V. Kumar, M.K. Sunkara, Adv. Func. Mat., 18, 2411 (2008).
- [4] S.M. Yong, T. Nikolay, B.T. Ahn, D.K. Kim, J. Alloy. Comp., 547, 113 (2013).
- [5] A.L. Viet, R. Jose, M.V. Reddy, B.V.R. Chowdari, S. Ramakrishna, J. Phys. Chem. C, 114, 21795 (2010).
- [6] B. Tan, E. Toman, Y. Li, Y. Wu, J. Am. Chem. Soc., 129, 4162 (2007).
- [7] M.Y.A. Rahman, M.M. Salleh, I.A. Talib, M. Yahaya, A. Ahmad, Curr. Appl. Phys., 7, 446 (2007).
- [8] L. Miao, P. Jin, K. Kaneko, A. Terai, N. Nabatova-Gabain, S. Tanemura, Appl. Surf. Sci., 212, 255 (2003).
- [9] C. C. Hsieh, K. H. Wu, J. Y. Juang, T. M. Uen, J.-Y. Lin, Y. S. Gou, J. Appl. Phys., 92, 2318 (2002).
- [10] M.Dj. Bles'ic', Z.V. S'aponjic', J.M. Nedeljkovic', D.P. Uskokovic, Mater. Lett., 54, 298 (2002).
- [11] J. Yu, X. Zhao, Q. Zhao, Thin Solid Films, 379, 7 (2000).
- [12] J.-G. Yu, H.-G. Yu, B. Cheng, X.-J. Zhao, J. C. Yu, W.-K. Ho, J. Phys. Chem., B, 107, 13871 (2003).
- [13] E. Hosono, S. Fujihara, K. Kakiuchi, H. Imai, J. Am. Chem. Soc., 126, 7790 (2004).
- [14] Y. Liu, S. Yang, J. Hong, C. Sun, J. Hazardous Mater., 142, 208 (2007).
- [15] D. Reyes-Coronado, G. Rodríguez-Gattorno, M.E. Espinosa-Pesqueira, C. Cab, R. de Coss, G. Oskam, Nanotechnology, 19, 145605 (2008).
- [16] L. Roza, A.A. Umar, M.Y.A. Rahman, M.M. Salleh, Adv. Mater. Res., 364, 393 (2012).
- [17] A. S. Barnard, L. A. Curtiss, Nano Lett., 5, 1261 (2005).
- [18] V. Kandavelu, H.-S. Huang, J.-L. Jian, T.C.-K. Yang, K.-L. Wang, S.-T. Huang, Solar Energy, 83, 574 (2009).
- [19] M.Y.A. Rahman, A.A. Umar, L. Roza, M.M. Salleh, Russian J. Electrochem., 50, 1072 (2014).